JOURNAL OF SOLID STATE CHEMISTRY 79, 1–11 (1989)

Crystal and Magnetic Structures of $LiCoF_4$: The First Compound with a Dirutile Structure

P. LACORRE AND J. PANNETIER

ILL, Avenue des Martyrs, 156X Grenoble Cedex, France

F. AVERDUNK AND R. HOPPE

Institut fur Anorganische und Analytische Chemie, Justus Liebig Universitat, Heinrich Buff Ring 58, D 6300 Giessen, Federal Republic of Germany

AND G. FEREY*

Laboratoire des Fluorures (UA CNRS 449), Faculté des Sciences, Université du Maine, Route de Laval, 72017 Le Mans Cedex, France

Received June 3, 1988; in revised form September 16, 1988

The nuclear and magnetic structures of the antiferromagnet $LiCoF_4$ (T_N = 150(2) K) were solved by neutron powder diffraction at 170 and 2 K, respectively. The nuclear structure (R_I = 0.047) provides the first explicit example of a dirutile structure with a Li^+–Co^{3+} cationic ordering within the chains. In order to explain the magnetic properties, it can also be described from $(CoF_4)^-$ perovskite-like layers between which Li^+ ions are inserted. The relationship between dirutile and $AFeF_4$ structures is discussed. The magnetic cell is $2a$, b, c. After the refinement of the data at 2 K (R_{nuc} = 0.041; R_{mag} = 0.065), the moments of Co^{3+} (μ = 3.62(8) μ_B) are found in the (010) plane (G_x, A_y, G_z mode) of the monoclinic cell. In terms of perovskite layers, the moments, perpendicular to the planes, indicate a negative value of the anisotropy term of the spin Hamiltonian.

Introduction

LiF gives very few combinations with 3d transition metal fluorides; during many years, only Li_3MF_6 compounds were known. However, one of us (R.H.) recently synthesized $LiCoF_4$ (*1*), which was the first compound with LiF/MF_3 = 1/1. Its powder X-ray diffraction pattern was tentatively indexed in a monoclinic cell (a = 5.540(3) Å, b = 4.665(1) Å, c = 5.447(3) Å, β = 114.25(5)°, Z = 2, space group $P2_1/m$). Further, the structure of the Jahn–Teller Mn^{III} homologous compound was solved from single-crystal data in a different space group (*2, 3*). Because of the lack of single crystals of $LiCoF_4$, we decided to solve first its crystal structure from powder neutron diffraction which would provide an accurate refinement of Li positions, and then its magnetic structure.

The format of the paper is as follows: in a

* To whom correspondence should be addressed.

0022-4596/89 $3.00

first part, we shall describe the experimental procedures; the second part will be devoted to the crystal structure determination of $LiCoF_4$ and the structural correlations with other fluorides. Finally, the magnetic properties and the magnetic structure which explains them will be presented.

Experimental

Powder sample of $LiCoF_4$ has been prepared for the first time by heating a mixture of stoichiometric amounts of lithium chloride and Co^{III} hexamine chloride under fluorine, deluted by nitrogen ($1F_2 : 5N_2$), at 400–420°C for 7 hr (*1*).

For the following investigations, $LiCoF_4$ has been synthesized by high-pressure fluorination of a LiF/CoF_2 mixture (both Merck, p.a.) in molar ratio 1 : 1 (1 day, 400°C, 300 bars). The pale purple samples are moisture sensitive. Only small amounts of CoF_3 have been observed on X-ray powder photographs.

Between 4.2 and 300 K, the magnetic susceptibility was measured by the Faraday method.

Neutron diffraction patterns were collected on the D1B powder diffractometer of the high-flux reactor of the Institut Laue-Langevin at Grenoble, using a wavelength of 2.157 Å. The diffractometer is equipped with a position-sensitive detector (PSD) which records simultaneously 80° in 2θ of the powder diffraction pattern. The sample was contained in a cylindrical vanadium can (diameter 10 mm) held in a vanadium tailed liquid helium cryostat. The absence of diffraction peaks at very low angles was first checked during a preliminary run at 2 K in the range $4° < 2\theta < 84°$. The PSD was then positioned to record the diffraction pattern in the range $23° < 2\theta < 103°$. The patterns were collected at various temperatures between 2 K and the Néel temperature in order to possibly detect anomalies in the thermal evolution of the magnetic moment. Finally, a longer data acquisition was performed above T_N, at 170 K, to record the pattern in the paramagnetic state, and therefore to solve the crystal structure of $LiCoF_4$.

The diffraction patterns were analyzed by the Rietveld method (*4*) as modified by Hewat (*5*). The nuclear scattering lengths and magnetic form factors were taken from Koester and Rauch (*6*) and Watson and Freeman (*7*), respectively. Bertaut's (*8*) representation theory was used to identify the possible models of magnetic structure.

Crystal Structure of $LiCoF_4$ at 170 K: Structural Correlations with Other AMF_4 Structures

The data are consistent with a monoclinic cell with the same space group as $LiMnF_4$: $P2_1/c$. Starting from the corresponding atomic coordinates, the refinement with isotropic temperature factors fixed at 0.1 $Å^2$ rapidly converged to the values of Table I ($R_I = 0.047$, $R_P = 0.073$, $R_{wp} = 0.081$). The comparison between observed and calculated intensities is illustrated by the pattern of Fig. 1a. Table II presents the corre-

TABLE I

REFINED CELL PARAMETERS AND ATOMIC COORDINATES OF $LiCoF_4$ (SPACE GROUP $P2_1/c$ (NO. 14), $Z = 2$) AT 170 K AND 2 K (VALUES AT 2 K ARE IN PARENTHESES)

a = 5.4354 (7) Å	(5.4296(8))	
b = 4.6527(6) Å	(4.6462(4))	
c = 5.5392(7) Å	(5.5371(4))	
β = 114.177(8)°	(114.244(5))	
V = 127.80(5) $Å^3$	(127.36(4))	

Atom site	x	y	z	B
Li (2b)	½	½	0	0.1
Co (2a)	0	0	0	0.1
F1 (4e)	0.8532(9)	0.7948(12)	0.6684(9)	0.1
	(0.8532(4))	(0.7924(10))	(0.6668(9))	(0.1)
F2 (4e)	0.3246(9)	0.6853(10)	0.6213(11)	0.1
	(0.3249(3))	(0.6844(8))	(0.6239(9))	(0.1)

Note. $R_I = 4.71\%$ (4.79%); $R_{prof} = 7.32\%$ (6.9)%); $R_{wprof} = 8.16\%$ (7.04%).

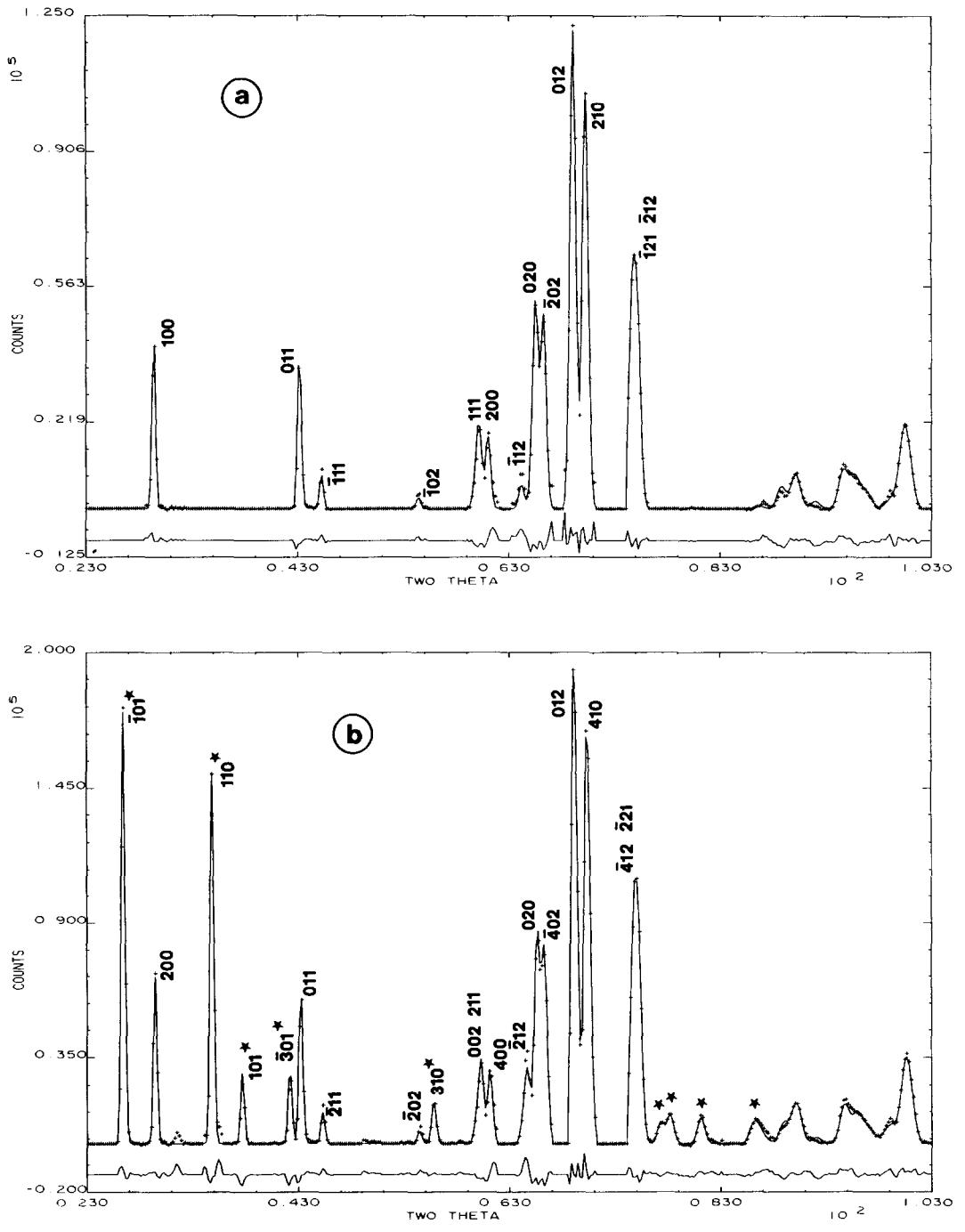

FIG. 1. Comparison between observed and calculated intensities of the diffraction peaks in the paramagnetic (170 K (a)) and ordered magnetic state (2 K (b)). The bottom line is the difference pattern at the same scale. The Miller indices of (b) refer to the magnetic cell $2a$, b, c. Magnetic peaks are identified by stars. For sake of clarity, hkl have been omitted above $2\theta > 78°$.

TABLE II

CHARACTERISTIC BOND LENGTHS (Å) AND ANGLES (°) IN $LiCoF_4$ AT 170 K AND 2 K (IN PARENTHESES)

		Co^{3+} octahedron		
Co–F11	2 × 1.929(5)	(1.931)	F11–Co–F13	89.06 (89.06)
Co–F13	2 × 1.999(6)	(1.992)	F12–Co–F13	90.94 (90.94)
Co–F23	2 × 1.827(5)	(1.823)	F11–Co–F23	85.58 (85.36)
⟨Co–F⟩	1.918	(1.915)	F11–Co–F24	94.42 (94.64)
			F13–Co–F23	90.81 (90.84)
			F13–Co–F24	89.19 (89.16)
F11–F13 = F12–F14 = 2.755(8) (2.751)			F11–F14 = F12–F13 = 2.801(8) (2.796)	
F11–F23 = F12–F24 = 2.552(7) (2.546)			F13–F23 = F14–F24 = 2.727(8) (2.720)	
F11–F24 = F12–F23 = 2.757(8) (2.761)			F13–F24 = F14–F23 = 2.689(7) (2.680)	
⟨F–F⟩ = 2.713 Å				
		Li^+ octahedron		
Li–F14	2 × 2.000(6)	(2.003)	F13–Li–F21	76.93 (77.02)
Li–F21	2 × 2.101(7)	(2.085)	F13–Li–F22	103.07 (102.98)
Li–F23	2 × 2.007(6)	(2.015)	F13–Li–F23	89.58 (89.18)
⟨Li–F⟩	2.036	(2.034)	F13–Li–F24	90.42 (90.82)
			F22–Li–F23	87.21 (87.47)
			F22–Li–F24	92.79 (92.53)
F13–F21 = F14–F22 = 2.552(7) (2.546)			F13–F24 = F14–F23 = 2.844(8) (2.861)	
F13–F22 = F14–F21 = 3.212(8) (3.199)			F21–F24 = F22–F23 = 2.834(8) (2.835)	
F13–F23 = F14–F24 = 2.823(8) (2.821)			F21–F23 = F22–F24 = 2.975(8) (2.963)	
⟨F–F⟩ = 2.873 Å				
		Metal–metal distances and superexchange angle		
Co–Co		3.617(2) (3.614)	Co1–Li1:3.577(1) (3.573)	
Co–F1–Co		134.06(21) (139.98)	Co1–Li2:2.982(1) (2.977)	

Note. In this table, two numbers define each fluorine. The first refers to the type of fluorine in Table I. The second corresponds to the coordinates of a Wyckoff position: 1, x, y, z; 2, $\bar{x}, \bar{y}, \bar{z}$; 3, $\bar{x}, \frac{1}{2} + y, \frac{1}{2} - z$; 4, $x, \frac{1}{2} - y, \frac{1}{2} + z$.

sponding bond lengths and characteristic angles; both Co^{3+} and Li^+ are octahedrally coordinated, with a somewhat large distortion of the Co^{3+} polyhedra. However, the mean distances are in excellent agreement with Shannon's ionic radii (*9*).

The corresponding (010) projection appears in Fig. 2. Co^{3+} and Li^+ ions lie in the (100) and (200) planes, respectively. This led to two descriptions of the structure. The first is deduced from the observation of the structure along [101]. In this direction, edge-sharing octahedra of Co^{3+} and Li^+ alternate, thus forming a rutile-like structure, the periodicity of which is twice that of the true rutile structure along its **c** axis (Fig. 3). This explains the denomination of *dirutile* that we claimed in the title, by comparison with the trirutile structure (*10*), commonly encountered both in oxides and fluorides (*11*). To our knowledge (*3*), this is the first explicit mention of such a structural type in the literature.

The cell vectorial relationship between the rutile structure (a_R, c_R), the dirutile (a_{2R}, b_{2R}, c_{2R}), and the true monoclinic cell are

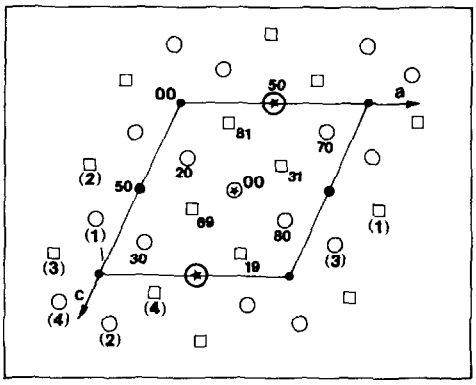

FIG. 2. (010) projection of $LiCoF_4$. Cobalt ions are represented as black circles, Li ions by circled stars, and fluorine F1 and F2 by open circles and squares, respectively. The y coordinates are indicated by a two-figure number (hundredth of the parameter). The single numerals (in parentheses) below F1 and F2 refer to the second number used to define the coordinates within a Wyckoff position (see Table II).

the following (Fig. 4):

$$\begin{vmatrix} a_{2R} \\ b_{2R} \\ c_{2R} \end{vmatrix} = \begin{vmatrix} 1\,0\,0 \\ 0\,2\,0 \\ 0\,0\,2 \end{vmatrix} \cdot \begin{vmatrix} a_R \\ b_R \\ c_R \end{vmatrix} = \begin{vmatrix} 0\,1\,0 \\ \bar{1}\,0\,1 \\ 1\,0\,1 \end{vmatrix} \cdot \begin{vmatrix} a_m \\ b_m \\ c_m \end{vmatrix} \quad (1)$$

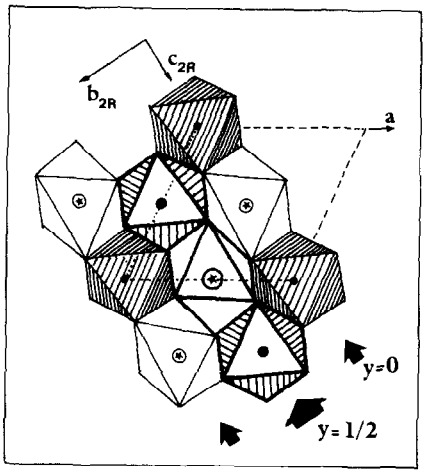

FIG. 3. Polyhedral representation in the (010) plane, showing the rutile-like arrangement.

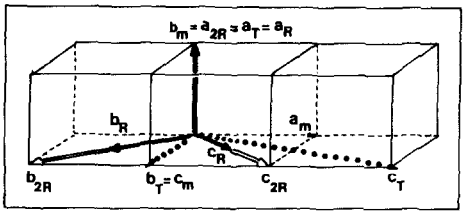

FIG. 4. Cell relations between the monoclinic Li CoF_4 (m indices), ideal rutile (R indices), dirutile (2R indices), and SnF_4 (T indices) structures.

Because of the cationic ordering between Co^{3+} and Li^+ also along the b_R direction, the b_{2R} axis is also doubled with respect to the rutile cell (Fig. 5).

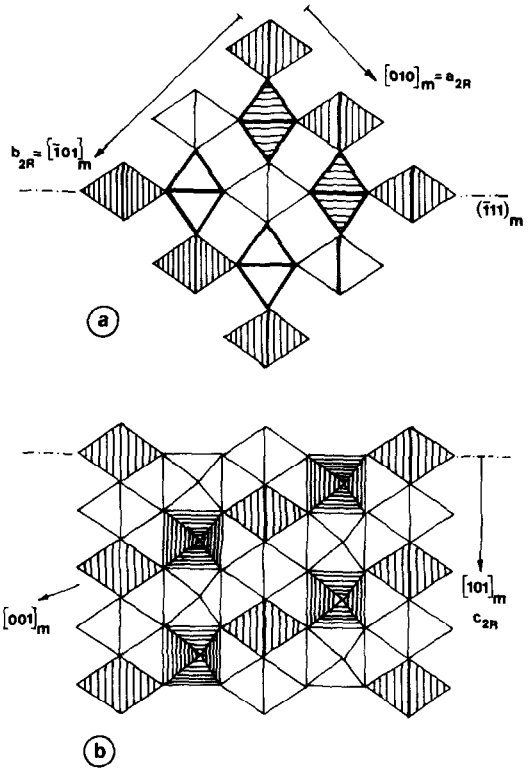

FIG. 5. (a) $LiCoF_4$ described as a rutile structure from the $[101]_m$ projection. Co^{3+} octahedra are hatched. The cationic ordering obliges to double the b parameter of the common rutile cell. (b) The projection on the $(111)_m$ plane shows the sequence of edge-sharing octahedra in $LiCoF_4$.

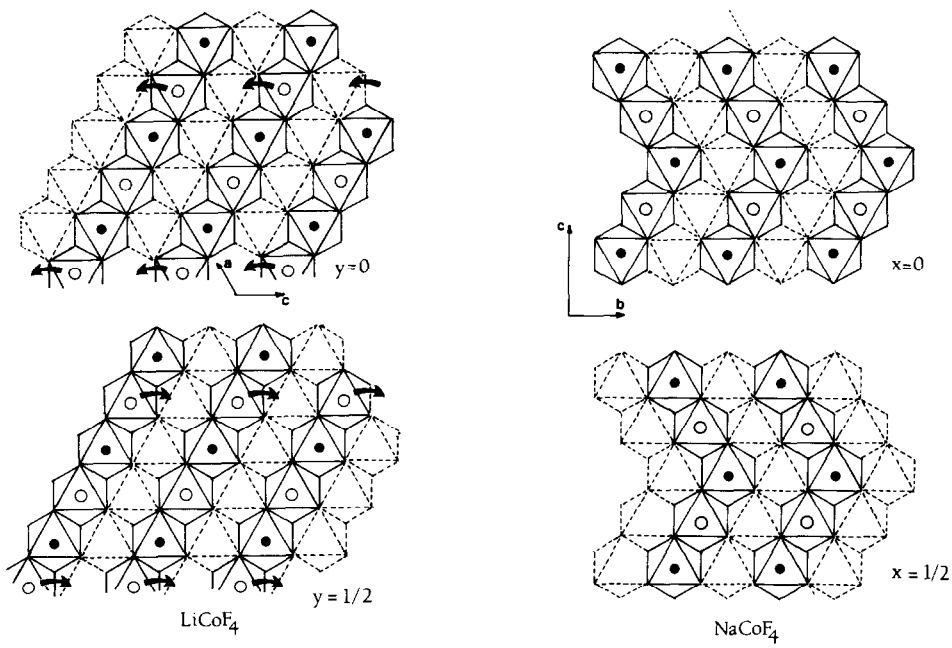

FIG. 6. Idealized (100) projection of $NaCoF_4$ (left) and (010) projection of $LiCoF_4$ (right) structures. They both adopt the *hc* packing for fluorine ions and differ only by the ordering of A^+/Co^{3+} cations. Arrows visualize the transformation from a structure to the other.

From this description, an interesting comparison between $LiCoF_4$ and $NaCoF_4$ (*1*), which is isostructural with $NaTiF_4$ (*12*), can be made. The orthorhombic structure of the latter can be described (Fig. 6) from connected layers, inside which appears a cationic ordering between Co^{3+} and Na^+, both in octahedral coordination. The octahedra share edges in the planes and draw zigzag chains which nicely illustrate the concept of "chemical twinning" proposed by Andersson and Hyde (*13*). Two chains within a layer are separated by octahedral vacancies which run in the same direction as the chains. The two structures are simply related by a shift of half the Li atoms to a neighbor vacancy, either parallel to the *hcp* plane of anions (through tetrahedral positions) or perpendicular to these planes (i.e., a move through a face of the octahedra).

The second description of the structure emphasizes the Co^{3+} octahedral subnetwork. In the (100) plane, cobalt ions build up (Fig. 7) a planar $(CoF_4)^-$ perovskite-like network of tilted corner-

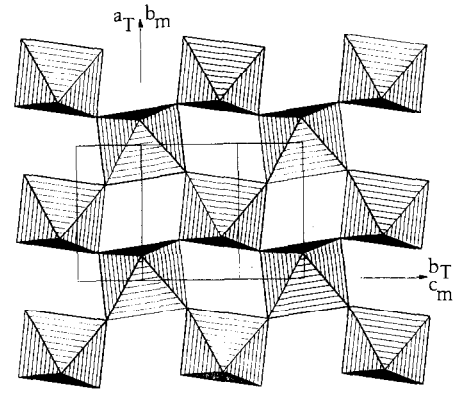

FIG. 7. $(100)_m$ projection of $LiCoF_4$ neutrons, 170 K (drawn using program STRUPLO (*15*)), illustrating the occurrence of tilted perovskite network of COF_6 octahedra.

sharing octahedra and draw a pseudotetragonal cell (a_T, b_T, c_T) related to the true monoclinic one by the relation:

$$\begin{vmatrix} a_T \\ b_T \\ c_T \end{vmatrix} = \begin{vmatrix} 0\ 1\ 0 \\ 0\ 0\ 1 \\ 2\ 0\ 1 \end{vmatrix} \cdot \begin{vmatrix} a_m \\ b_m \\ c_m \end{vmatrix} \qquad (2)$$

This crystal chemistry was already encountered in SnF_4 (*14*) and in many AMF_4 compounds with A = K, Rb, Cs and M = Al, Fe, Co, T, V (see for instance Ref. (*11*) for a review of these structures). If we describe the latter compounds in the cell a_T, b_T, c_T, the perovskite layers are either staggered (with A = Rb, Cs), or shifted (A = K) one toward the other by a vector $(-\frac{1}{4}, \frac{1}{4}, \frac{1}{2})$. In this description, which will prove to be of interest for the study of the magnetic properties, $LiCoF_4$ and $NaTiF_4$ exhibit a new type of shift between the perovskite layers (vector $0, \frac{1}{2}, \frac{1}{2}$) in the AMF_4 family, whereas it has already been encountered in the SnF_4-type and K_2NiF_4-type structures.

However, in the planes of $LiCoF_4$, the tilting of the octahedra is much more pronounced than in the other related structures and leads to low superexchange angles Co–F–Co (134.06°) compared to the values of about 150° usually found in this type of structure. This large tilting enables us to explain the transformation from the SnF_4 structure to the dirutile structure in which the alkali ion exhibits the octahedral coordination, and finally to the distorted $TlAlF_4$-type structure. The insertion into the SnF_4-type structure of small cations such as Li or Na, which commonly adopt a sixfold coordination, induces a rotation of the octahedra, indicated in Fig. 8 by arrows. The substitution by larger K^+ leads to a shift of the MF_4 layers because of the higher coordination number of K^+. This mechanism suggests that high pressures—which usually increase the coordination of the ions—could transform $LiCoF_4$ into a $TlAlF_4$-related structure.

TABLE III

RUTILE AND PSEUDOTETRAGONAL CELL PARAMETERS AS CALCULATED FROM EQS. (1) AND (2) AT 170 K (MONOCLINIC DESCRIPTION)

Rutile	Pseudotetragonal
a_R = 4.6527 Å	a_T = 4.6527 Å
b_R = 4.6068 Å	b_T = 5.5392 Å
c_R = 2.9818 Å	c_T = 9.9767 Å
α_R = 91.188°	γ_T = 96.255°

The dirutile description of $LiCoF_4$ is crystallographically more accurate than the layer one. The calculation of the cell parameters from Eqs. (1) and (2) leads to the results given in Table III: the deviation from an ideal tetragonal cell is less than 1.5% for the rutile description but much larger for the layered perovskite description. This is confirmed by the Co–F–Co angle (134.06°) which is even smaller than the Ti–F–Ti angle in α-$NaTiF_4$ (140°) (*12*), and very close to the M–F–M angles in rutile (typically 132°). On the other hand, in addition to their large tilting, the perovskite layers are not perfectly stacked on top of each other: the shift between the c_T axis and perpendicular to the perovskite plane is about 6.25°. A similar effect is observed in α-

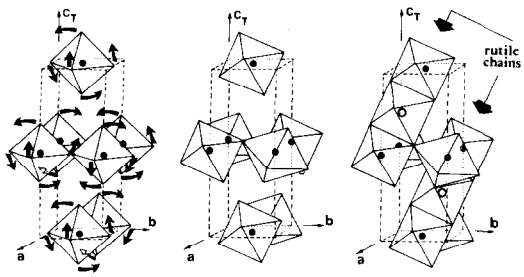

FIG. 8. Illustration of the geometrical transformation from the SnF_4-type structure (left) to the dirutile (right) by cooperative rotation of octahedra in each plane (center). For the sake of clarity, the a and b axes on the figure correspond to $\frac{1}{2}(a_T + b_T)$ and $\frac{1}{2}(a_T - b_T)$, respectively.

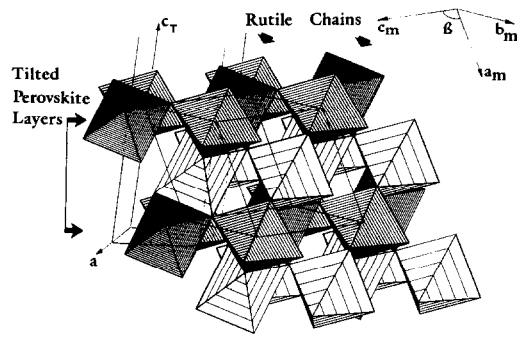

FIG. 9. Perspective view of $LiCoF_4$ neutrons (*15*), 170 K, showing both the tilted perovskite layers of Co^{3+} octahedra (heavily hatched) and the ordered rutile chains. Li^+ octahedra are lightly shaded. The *a* parameter of the tetragonal cell is defined as in Fig. 8.

$NaTiF_4$. The perspective view of $LiCoF_4$ (Fig. 9) summarizes the two possible descriptions of the structure.

The Madelung Part of Lattice Energies, MAPLE (*16*)

In Table IV, we compare MAPLE of Li CoF_4 with the sum of the MAPLE values of LiF and CoF_3. The agreement is not very satisfactory, but MAPLE of CoF_3 is based on a structural proposal derived from powder data (*17*), in which *d*(Co–F) is 1.89 Å. Alternatively, using the relation,

$$\begin{matrix} \text{MAPLE}(LiCoF_4) & - & \text{MAPLE}(LiF) \\ 1819.1 & & 288.7 \end{matrix} = \text{MAPLE}(CoF_3)$$
$$1530.4 \text{ kcal/mole},$$

one obtains for CoF_3 a value for MAPLE which corresponds to *d*(Co–F) = 1.933 Å. This distance agrees not only with the mean value *d*(Co–F) in $LiCoF_4$ (1.918 Å), but also with the estimated Co–F distance in $LiSrCoF_6$ (1.92 Å) which was derived by comparison (*18*) with the structure of LiSr FeF_6 (*19*), determined from single-crystal data. This distance corresponds to a MAPLE value of 1540 kcal/mole for CoF_3.

TABLE IV

MAPLE VALUES OF $LiCoF_4$ IN KILOCALORIES PER MOLE

		Binary	Ternary	Δ[c]	Δ
Li^+	1×	1.44.3[a]	165.9	+21.6	+21.6
Co^{3+}	1×	1083.3[b]	1039.0	−44.3	−44.3
$F^-(1)$	1×	144.3[a]	167.9	+23.6	+23.6
$F^-(1)$	1×	160.1[b]	167.9	+ 7.8	+ 7.8
$F^-(2)$	2×	160.1[b]	139.2	−20.9	−41.8
Σ		1852.2	1819.1		−33.1[d]
					≙ −1.78%

[a] From LiF.
[b] From CoF_3.
[c] (Δ) Ternary–binary.
[d] (ΣΔ) $MAPLE_{(LiCoF_4)} - MAPLE_{(LiF)} - MAPLE_{(CoF_3)}$.

Magnetic Structure of $LiCoF_4$

The thermal variation of the reciprocal magnetic susceptibility is shown in Fig. 10. Even at room temperature, the Curie–Weiss law is not obeyed and it was not possible to determine a significant value of θ_p; it is however strongly negative, in agreement with the antiferromagnetic structure described below. $\chi^{-1}(T)$ has a minimum at 150(5) K, increases to 82 K, and decreases below this temperature. At every temperature, the susceptibility is very weakly field

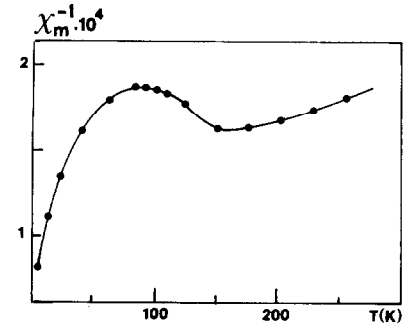

FIG. 10. Thermal evolution of the reciprocal susceptibility of $LiCoF_4$.

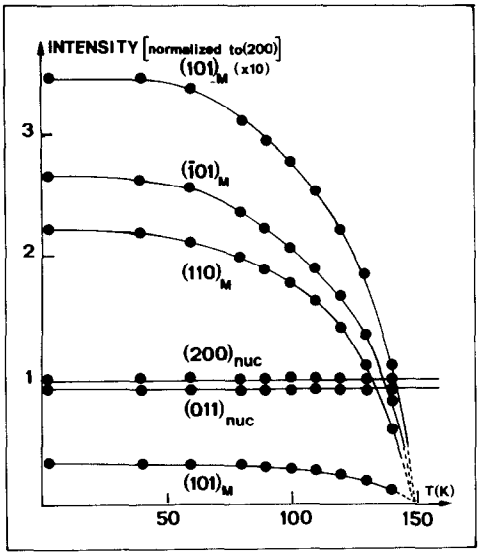

FIG. 11. Thermal evolution of the intensity of some magnetic peaks (normalized to the intensity of the nonmagnetic reflection (200)). The intensity variation indicates that the Néel temperature is 150 K and corresponds to the local minimum of $\chi^{-1}(T)$.

dependent. This is due to the small amounts of CoF_3 (T_N = 393 K) present in the sample.

From the neutron diffraction patterns collected at various temperatures in the range 2–170 K (Fig. 11), it is possible to determine the thermal evolution of the intensity of some magnetic peaks. This indicates that the Néel temperature corresponds to the minimum of $\chi^{-1}(T)$ observed at 150 K. Below this temperature, new purely magnetic peaks appear. These new peaks imply the doubling of the a parameter of the paramagnetic cell. The magnetic cell thereby contains four Co^{3+} ions and the propagation vector (7) is then $k = [\frac{1}{2}\ 0\ 0]$.

Using Bertaut's theory, and defining as S_i (i = 1, 4) the magnetic moments of Co^{3+} corresponding to the atomic coordinates reported in Table V, it is possible to use four linear combinations of the moments $F = S_1 + S_2 + S_3 + S_4$, $G = S_1 - S_2 + S_3 - S_4$, $C = S_1 + S_2 - S_3 - S_4$, $A = S_1 - S_2 - S_3 + S_4$ which represent the ferromagnetic and antiferromagnetic modes of coupling. The base vectors, in the irreducible representation of space group $P2_1/c$ lead to the four modes indicated in Table V.

TABLE V

COORDINATES OF THE MAGNETIC IONS Co^{3+} AND IRREDUCIBLE REPRESENTATION IN THE $P2_{1/c}$ SPACE GROUP

S_1	0	0	0
S_2	$\frac{1}{2}$	0	0
S_3	$\frac{1}{2}$	$\frac{1}{2}$	$\frac{1}{2}$
S_4	0	$\frac{1}{2}$	$\frac{1}{2}$

Mode	x	y	z
Γ_1 (++)	A_x	G_y	A_z
Γ_2 (+−)	C_x	F_y	C_z
Γ_3 (−+)	F_x	C_y	F_z
Γ_4 (+−)	G_x	A_y	G_z

Atomic coordinates and spin components were refined simultaneously. The best fit (R_{mag} = 0.065) between observed and calculated intensities (a list can be obtained on request to G.F.) corresponds to the Γ_4 mode. The components of the magnetic moments on the axes of the cell are listed in Table VI; atomic coordinates are indicated in parentheses in Table I. The comparison between observed and calculated profiles is given in Fig. 1b. The spins of Co^{3+} (μ = 3.62(8)μ_B) lie in the (010) planes of the monoclinic cell (Fig. 12). The doubling of the a parameter of the nuclear cell results

TABLE VI

REFINED MAGNETIC MOMENTS (IN μ_B) AT 2 K

Atom	M_x	M_y	M_z	M
S_1	−3.94(2)	0	−2.10(5)	−3.62(9)
S_2	3.94(2)	0	2.10(5)	3.62(9)
S_3	−3.94(2)	0	−2.10(5)	−3.62(9)
S_4	3.94(2)	0	2.10(5)	3.62(9)

Note. R_{nuc} = 4.12%; R_{mag} = 6.47%; R_{prof} = 6.90%; R_{wp} = 7.04%; R_{exp} = 1.03%.

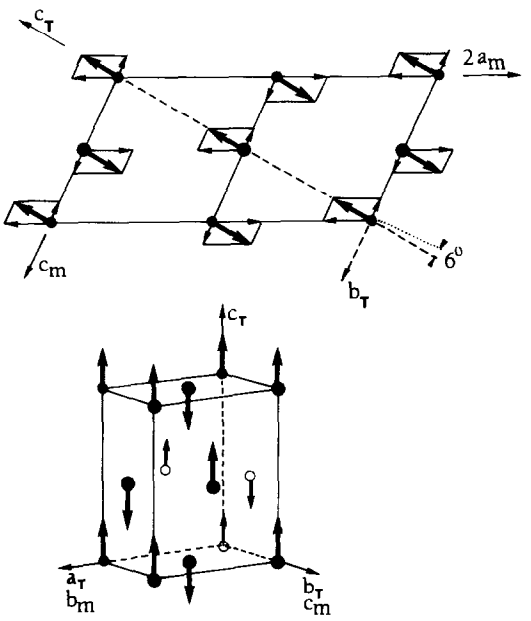

FIG. 12. Magnetic structure of $LiCoF_4$. The moments are strictly colinear to [101] direction of the monoclinic cell, and roughly perpendicular to its (b_m, c_m) perovskite-like plane.

from the antiferromagnetic coupling of S_1 and S_2. Within the perovskite layers, the spins adopt the *G*-type arrangement, commonly observed in this type of structure.

At variance with the crystallographic description, the spin arrangement is more easily described in the pseudotetragonal cell of the distorted perovskite layer model. When compared to other rutiles such as MnF_2, FeF_2, or CoF_2, the c_R axis is no longer a direction of easy magnetization. On the contrary, magnetic moments are aligned with the c_T axis of the pseudotetragonal cell, i.e., with a slight disorientation of about 6° with respect perpendicular to the perovskite plane (Fig. 12).

The quasiorthogonality between the direction of the spins of Co^{3+} (d^6) and the perovskite plane must be underlined and compared to the situation previously encountered for isoelectronic compounds K_2FeF_4 and Ba_2FeF_6 (*20*). Both of them contain perovskite layers as $LiCoF_4$ but, whereas the moments lie in the layers for K_2FeF_4, they are orthogonal to them for Ba_2FeF_6. Mössbauer spectroscopy has shown (*21*) that these different situations are related to the magnetic anisotropy of d^6 ions. The latter can have two origins: magnetocrystalline (DS_z^2 term of the spin Hamiltonian) or dipolar magnetic. We have shown that D is positive (easy plane of magnetization) for K_2FeF_4 and negative (easy axis of magnetization) in Ba_2FeF_6. Because of the sign of D, the two types of anisotropy act in the same way (axial magnetization) in Ba_2FeF_6, whereas they are opposite in K_2FeF_4. As the crystalline anisotropy is larger than the dipolar one, the moments lie in the plane in K_2FeF_4. From this point of view, the behavior of $LiCoF_4$ is more closely related to that of Ba_2FeF_6 ($D < 0$) rather than that of K_2FeF_4 ($D > 0$).

Finally, it will be of some interest to compare in the near future the evolution of the magnetic properties with the various superstructures of the rutile family (mono-, di-, and trirutile), keeping constant the chemical nature of the magnetic cation.

References

1. T. FLEISCHER AND R. HOPPE, *Z. Naturforsch. B* **37,** 1132 (1982).
2. K. H. WANDNER AND R. HOPPE, *Z. Anorg. Allg. Chem.* **546,** 113 (1987).
3. R. HOPPE, *Z. Anorg. Allg. Chem.* **554,** 240 (1987).
4. H. M. RIETVELD, *J. Appl. Crystallogr.* **2,** 65 (1969).
5. A. W. HEWAT, Harwell Report AERE, R 7350 (1973).
6. L. KOESTER AND H. RAUCH, IAEA Contract 2517/RB (1981).
7. R. E. WATSON AND J. FREEMAN, *Acta Crystallogr.* **14,** 27 (1961).
8. E. F. BERTAUT, *in* "Magnetism III" (T. Rado and E. Shull, Eds.) (1963).
9. R. D. SHANNON, *Acta Crystallogr. A* **32,** 751 (1976).
10. A. BYSTROM, B. HOL, AND B. MASON, *Ark. Kemi Mineral. Geol. B* **15,** 4 (1941).

11. D. BABEL AND A. TRESSAUD, *in* "Inorganic Fluorides" (P. Hagenmuller, Ed.), p. 77, Academic Press (1985).
12. J. OMALY, P. BATAIL, D. GRANDJEAN, D. AVIGNANT, AND J. C. COUSSEINS, *Acta Crystallogr. B* **32,** 2106 (1976).
13. S. ANDERSSON AND B. G. HYDE, *J. Solid State Chem.* **9,** 92 (1974).
14. R. HOPPE, *Naturwissenschaften* **49,** 254 (1962).
15. R. X. FISCHER, *J. Appl. Crystallogr.* **18,** 258 (1985).
16. R. HOPPE, *Z. Anorg. Allg. Chem.* **283,** 196 (1956); *Angew. Chem.* **78,** 52 (1966); *Angew. Chem.* **82,** 7 (1970); *Adv. Fluorine Chem.* **6,** 387 (1970); *Izvjestaj Jugoslav. Centr. Kristallogr.* **8,** 21 (1973); "Crystal Structure and Chemical Bonding in Inorganic Chemistry," pp. 127–161, Amsterdam (1975).
17. M. A. HEPWORTH, K. H. JACK, R. D. PEACOCK, AND G. J. WESTLAND, *Acta Crystallogr.* **10,** 63 (1957).
18. T. FLEISCHER AND R. HOPPE, *Z. Naturforsch. B* **37,** 988 (1982).
19. T. FLEISCHER AND R. HOPPE, *Z. Naturforsch. B* **37,** 981 (1982).
20. J. RENAUDIN, J. PANNETIER, S. PELAUD, A. DUCOURET, F. VARRET, AND G. FEREY, *Solid State Commun.* **47,** 445 (1983).
21. S. PELAUD, Thèse de 3 ème Cycle, Le Mans (1983).